Available online at www.sciencedirect.com

SciVerse ScienceDirect

Ceramics International 38 (2012) 2813–2821

CERAMICS INTERNATIONAL

www.elsevier.com/locate/ceramint

Sol–gel preparation and characterization of nano-crystalline lithium–mica glass–ceramic

M.R. Tohidifar [a], P. Alizadeh [a,*], P. Riello [b], B. Eftekhari-yekta [c], A.R. Aghaei [d]

[a] Department of Materials Science and Engineering, Tarbiat Modares University, P.O. Box 14115-143, Tehran, Iran
[b] Department of Molecular Sciences and Nanosystems, University of Ca'Foscari, Venice, Italy
[c] Department of Materials Engineering, Iran University of Science and Technology, Tehran, Iran
[d] Ceramic Division, Materials and Energy Research Center, Tehran, Iran

Received 5 November 2011; received in revised form 13 November 2011; accepted 18 November 2011
Available online 28 November 2011

Abstract

The nano-crystalline lithium–mica glass–ceramic with separated crystallite size of 13 nm was prepared using sol–gel technique. In such a process, the structural evolutions and microstructural characteristics of the synthesized samples were investigated through X-ray diffraction, transmission electron microscopy, thermal analysis and Fourier transform infrared spectroscopy. It was found that the crystallite size of the mica obtained from sol–gel method is smaller than the one synthesized via conventional melted method. The XRD results also showed that the crystallization of mica occurred above 675 °C and it could originate from MgF_2 so that the next stage will also be the transformation from mica to norbergite and norbergite to chondrodite. The activation energy of the crystallization and Avrami factor were measured as 376.7 kJ mol^{-1} and 2.3, respectively. It is found that the bulk crystallization could be considered as the predominant crystallization mechanism for the glass–ceramic.

Keywords: A. Sol–gel processes; A. Calcination; B. Electron microscopy; D. Glass ceramics

1. Introduction

Glass–ceramics are polycrystalline ceramic materials, derived through the controlled nucleation and crystallization of glass, where the content of residual glassy phase is usually less than 50% [1,2]. Glass–ceramics have several advantages over conventional types of powder processed ceramics. In addition to the ease of flexibility of forming the glassy state, glass–ceramics have a uniformity of microstructure and reproducibility of glass [1–3]. Of the many types of obtainable microstructures in glass–ceramics, those based on uniformly dispersed crystals <100 nm in size provide unique attributes for the current products and offer promise for many potential new applications [3].

Mica glass–ceramics are such typical machinable ceramics where the crystals of mica disperse within a glassy matrix. Apart from being machinable, the mica-based glass–ceramics exhibit heat resistance exceeding 800 °C, electrical insulating properties as well as high mechanical strength [4–9].

Recently Taruta et al. [4,7] successfully prepared a novel mica glass–ceramics where the separated micas are lithium–mica type with a mean crystallite size of 20 nm in which the interlayer cation is lithium ion. Thus, the novel mica glass–ceramics have potential applications not merely as mechinable ceramics and optical materials but also as lithium ion conductors, practically used in many application fields [4,7].

In recent years, the glasses prepared through a sol–gel route are found to have advantages over conventional melted-quenching method such as: better homogeneity, higher level purity and lower stoichiometric losses [10–21]. On the other hand, it is generally accepted that the sol–gel rout enables to provide the transparent bulk glass–ceramic which can be very useful technique in the optical devices fabrication. Since, there is a technological interest in luminescent properties of transparent lithium–mica glass–ceramic [8] their sol–gel synthesis method can open technological possibilities in the wide range of this purpose. In addition, the mica glass–ceramic prepared by the sol–gel process can possess homogeneity that is

* Corresponding author. Tel.: +98 21 82884399; fax: +98 21 82883381.
E-mail address: p-alizadeh@modares.ac.ir (P. Alizadeh).

0272-8842/$36.00
doi:10.1016/j.ceramint.2011.11.052

particularly necessary for the machinable glass–ceramics because an interlocked, randomly oriented uniform microstructure of mica crystals is responsible for their machinability and good strength [5,6].

Although there are a few articles that show is possible to lithiated mica by ion exchange from different melts [22,23], so far, no research has been reported in the area of lithium–mica sol–gel synthesis hence, the present investigation intends to prepare the nanocrystalline lithium–mica glass–ceramic applying the aqueous sol–gel process, to characterize the synthesized powders and compare it with the one provided by Taruta et al. through the conventional melted method.

2. Experimental procedure

2.1. Gel preparation

Chemicals used to prepare the precursor gels were reagent grade tetraethyl orthosilicate (TEOS, Merck), aluminum iso-propoxide (Merck), lithium nitrate (Merck), magnesium nitrate hexahydrate (Merck) and ammonium fluoride (Merck). Ethanol (Merck) and toluene (Merck) were used as solvents.

In the beginning, the materials were mixed in accordance with chemical compositions i.e. $Li_{(1+x)}Mg_3AlSi_{3(1+x)}O_{10+6.5x}F_2$ ($x = 0.5$) and 5.1 mass% MgF_2 for crystallizing a large quantity of the lithium–mica [4,7]. Considerably, SiO_2 and Li_2O components are used more than the stoichiometric fluorophlogopite type of lithium–mica ($LiMg_3AlSi_3O_{10}F_2$) [4]. Fig. 1 shows the flowchart of the synthesis process.

First, the calculated amount of $Mg(NO_3)_2{\cdot}6H_2O$ and $LiNO_3$ was dissolved stirring in ethyl alcohol (C_2H_5OH) and HNO_3 as a solvent and pH controller, respectively. The solution of $Mg(NO_3)_2{\cdot}6H_2O$, $LiNO_3$ and ethyl alcohol was called solution A. The pH of solution A was adjusted around values of 3–4. Calculated quantity of aluminum iso-propoxide (AIP) was then dissolved in toluene under stirring and named as solution B. In order to partially hydrolyze of TEOS, the calculated amount of TEOS was mixed with ethyl alcohol, distilled water and HNO_3 stirred at room temperature of about 30 min, where the molar ratio of TEOS, distilled water and HNO_3 was kept at 1:4:0.05. The ethyl alcohol and TEOS were mixed with equal volume ratio. The solution C was also prepared from the appropriate proportion of NH_4F, distilled water, and HNO_3 as a fluorine source, solvent and pH controller, respectively. As such, the pH of solution C was kept around values of 1–2. The molar ratio of total chemicals and applied distilled water for the resolving of NH_4F was considered at 1:2.

After the solution A was stirred for 1 h, the solution B was added to it drop-wise using a burette on continuous stirring. Half an hour later, when the mixed solution became transparent, the pre-hydrolyzed TEOS was added to the above-mixed (A + B) solution and stirred for 10 min. Finally, the solution C was added drop-wise to the above mixed solution and the resulting homogeneous transparent solution was then stirred for about 4 h. The final pH range of the system was measured 2–3. The prepared sol was then poured into a glass beaker covered with aluminum foil and kept standing in the room temperature until it set to gel. The wet gel was transferred to a 110 °C oven and held there for 48 h. The dried gel was heated under different conditions to obtain glass–ceramic materials.

2.2. Thermal analyses

Thermal traces such as decomposition of residual organic materials or nitrate groups and crystallization for the Li_2O–MgO–Al_2O_3–SiO_2–F gel were conducted by using simultaneous DSC (differential scanning calorimetry) and TG (thermal gravimetry) method. This method was used in 25–1000 °C range with various heating rates (5, 10, 20 and 30 °C/min) with the STA instrument (Netzsch STA 409 C).

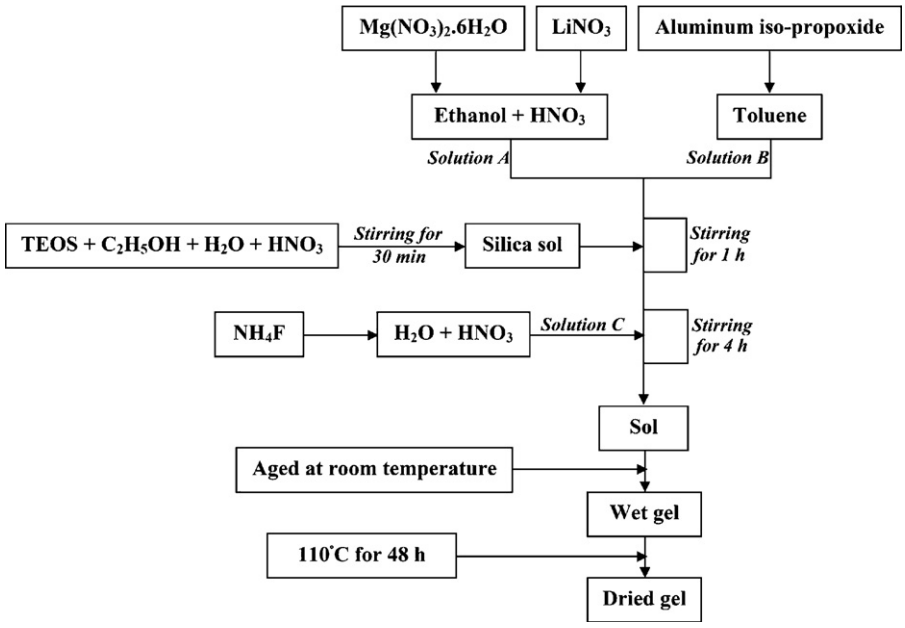

Fig. 1. The flow chart of lithium–mica synthesis applied sol–gel technique.

2.3. X-ray diffraction (XRD) analyses

X-ray diffraction was used for phase analysis of different samples employing Philips X-pert diffractometer with Co Kα radiation. The average crystallite size of mica was also estimated using the Scherrer formula [24].

2.4. Fourier transformation infrared spectroscopy

In order to investigate the chemical bonds of the samples, the Fourier transformation infrared spectroscopy (FTIR) experiments of various specimens (dried gel and heat treated specimens) were performed in a Nicolet Nexus 6700.

2.5. Transmission electron microscopy

Finally, the morphology and crystallite size of nanocrystalline mica were investigated by transmission electron microscopy (TEM) using a JEOL JEM-3010 microscope operated at 300 kV along with EDS spectra equipment for chemical analysis of the samples.

3. Results and discussion

3.1. Sol–gel process

The hydrolysis, polymerization and condensation procedures of chemicals cause the production of gel under convenient processing conditions. First, alkoxides and other chemicals may be hydrolyzed to prepare the sol. It is noticed that the applied chemicals in the current synthesis process were not hydrolyzed simultaneously, because the rate of hydrolysis reaction was different for each ion. In other words, the hydrolysis rate of a cation is strongly dependent on the synthesis condition i.e. pH of the system. So, only one ion may be hydrolyzed under specific applied conditions for solution. Since the pH of the system was adjusted around 2–3, the Si^{4+} cation could hydrolyzed alone in this pH range. In other words, the major role for hydrolysis and condensation process is attributed to the hydrolysis and condensation of TEOS. Other constituents were not hydrolyzed because the required pH value for hydrolysis was higher than this range. In the next stage, the Si–O Skelton was developed after the aggregation of TEOS hydrolyzed groups together and consequently other un-hydrolyzed ions entered into interstices of the silica gel structure [17].

3.2. Thermal behavior of the gel

Fig. 2 depicts DSC-TG diagram that shows several endothermic and exothermic peaks, with increasing gel temperature. The first of these peaks (endothermic peak) at 117 °C is attributed to the evaporation of remaining solvents (ethanol and water) in the gel structure and dehydration of the dried gel. The second peak at about 265 °C (exothermic peak) can be related to combustion of the residual organics materials originated from TEOS (tetraethyl orthosilicate) and AIP (aluminum iso-propoxide) components. Corresponding to this peak, a weight loss of 15% is observed in the TG diagram. The small exothermic peak is also detected at about 288 °C. This peak might be corresponding to the crystallization of MgF_2 which was confirmed by a later XRD analysis. An endothermic broadening peak is also observed at the temperature around 440 °C. This one

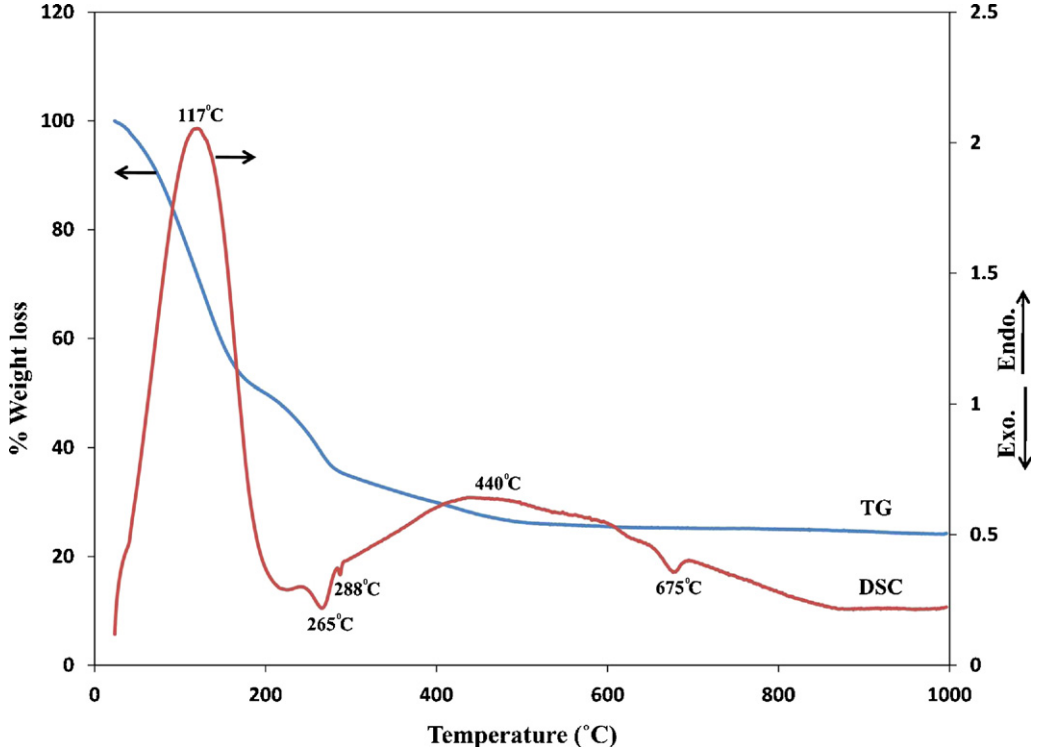

Fig. 2. DSC-TG curves for the gel of mica glass–ceramic.

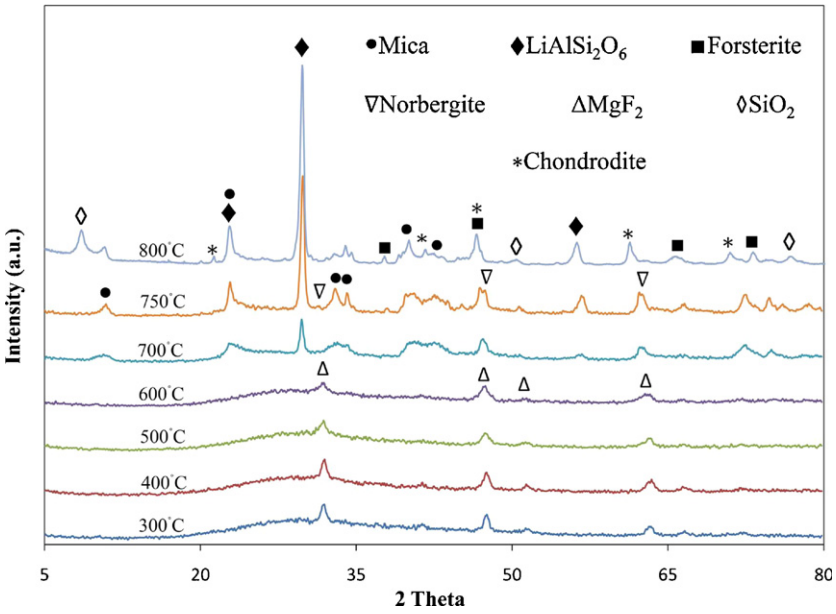

Fig. 3. The XRD patterns of the mica glass–ceramic heated at different temperatures for 0 h.

can be attributed to decomposition and removal of remaining nitrates ions introduced from magnesium and lithium nitrates. The TG diagram shows a 10% weight loss, corresponding to this stage. Apparently, no significant weight loss appears after about 500 °C. Finally, an exothermic peak is detected at 675 °C that can be related to the simultaneous crystallization of mica and lithium aluminum silicate as confirmed by later XRD technique. It is observed that a total weight loss of about 75% occurs in the dried gel after the heat treatment at 500 °C.

3.3. XRD analyses

X-ray diffraction (XRD) patterns of $Li_{(1+x)}Mg_3AlSi_{3(1+x)}O_{10+6.5x}F_2$ ($x = 0.5$) with 5.1 mass% of MgF_2 heat treated at different temperature for soaking time of 0 h, are presented in Fig. 3. As it can be seen, with increasing temperature from 300 °C, MgF_2 is only precipitated throughout amorphous system whereas at higher temperatures, MgF_2 is disappeared and the crystallization of the mica occurs at 675 °C along with some of the other phases (according to DSC diagram). It can be seen that the sample heat treated at 800 °C was composed of various undesirable phases so that it seems that the mica was decomposed to the other phases like chondrodite. The figure clearly shows that the temperature range of 700–750 °C should be considered as an appropriate range of temperature for promoting the mica crystallization because the mica is still stable as well as the less undesirable phases are developed at this range of temperature.

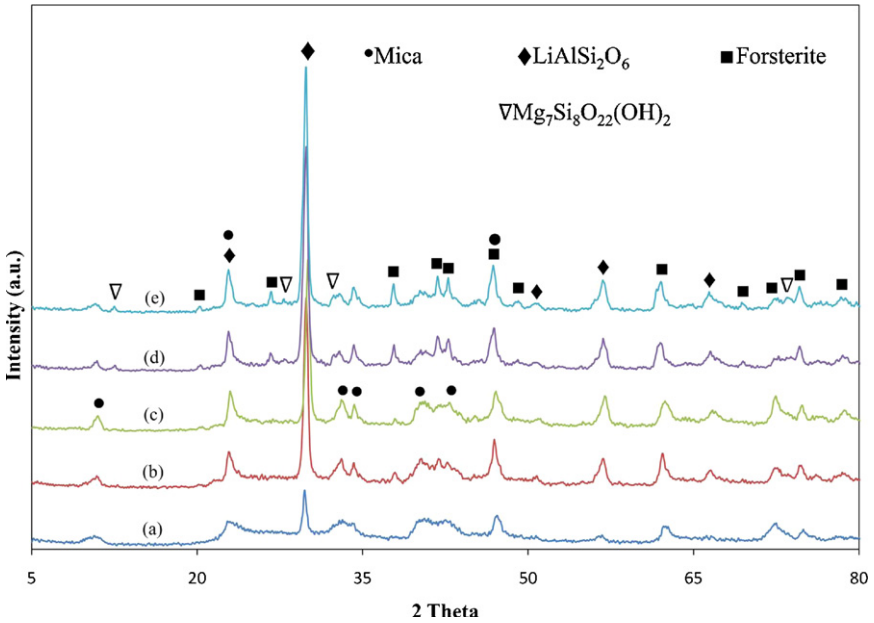

Fig. 4. The XRD patterns of the mica glass–ceramic heated at 700 °C for different heating times: (a) 0 h, (b) 2 h, (c) 4 h, (d) 6 h, and (e) 8 h.

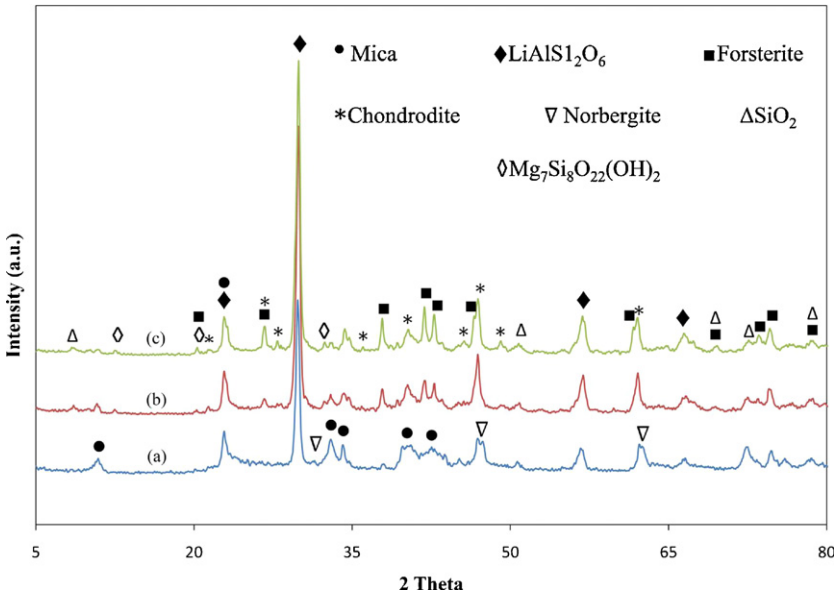

Fig. 5. The XRD patterns of the mica glass–ceramic heated at 750 °C for various heating times: (a) 0 h, (b) 2 h, and (c) 4 h.

Fig. 4 shows the X-ray diffraction patterns of the samples heat treated at 700 °C at different times. It is observed that the intensity of mica diffraction peaks are tailed off with increasing heating time (6 and 8 h) and undesirable phases such as $Mg_7Si_8O_{22}(OH)_2$ are formed consequently along with decomposing of the mica. It seems that the heating time of 4 h is appropriate for having stable mica phase through heat treatment of sol–gel powder derived at 700 °C.

Fig. 5 shows the XRD patterns of the samples heat treated at 750 °C for various times. The figure clearly reveals that the norbergite ($Mg_3SiO_4F_2$) phase is formed of the mica crystals when the heat treatment temperature is reached at 750 °C. The norbergite is also transformed to the chondrodite ($Mg_5(SiO_4)_2F_2$) when it takes a long time (2 and 4 h) to heat the gel. Taruta et al. [7] have reported that the chondrodite was formed before the mica, however XRD patterns demonstrate that the mica was originated from MgF_2 particles due to having compatible structures [6] as well as in the next stages the norbergite and chondrodite crystals were formed with increasing temperature and heating time, respectively. So, the difference in the sequences of the mica transformations is clearly observed based on the two different methods. Since, the synthesized mica via sol–gel method transforms to the two various phases (norbergite and chondrodite) it can be expected that the precipitated mica disappear earlier than the one synthesized by the melt-quenching method and consequently the optimized crystallization temperature range of mica (700–750 °C) is different to that prepared by melted method (650–800 °C) [4].

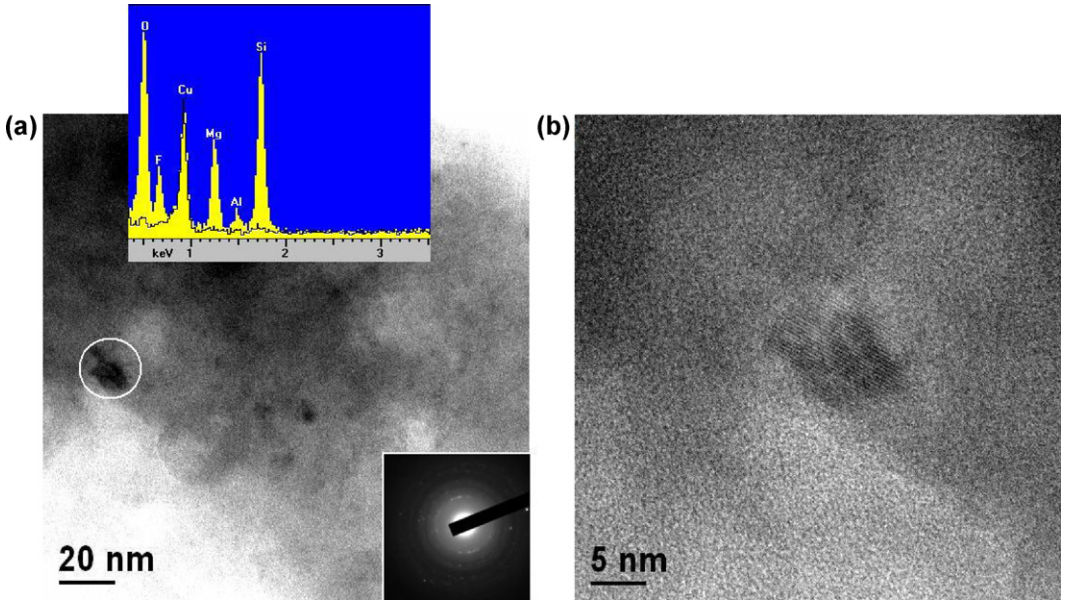

Fig. 6. TEM photograph of (a) the specimen heat treated at 700 °C and corresponding SAED pattern with the attached EDS spectra taken from the marked particle and (b) HRTEM image of mica nano-crystal.

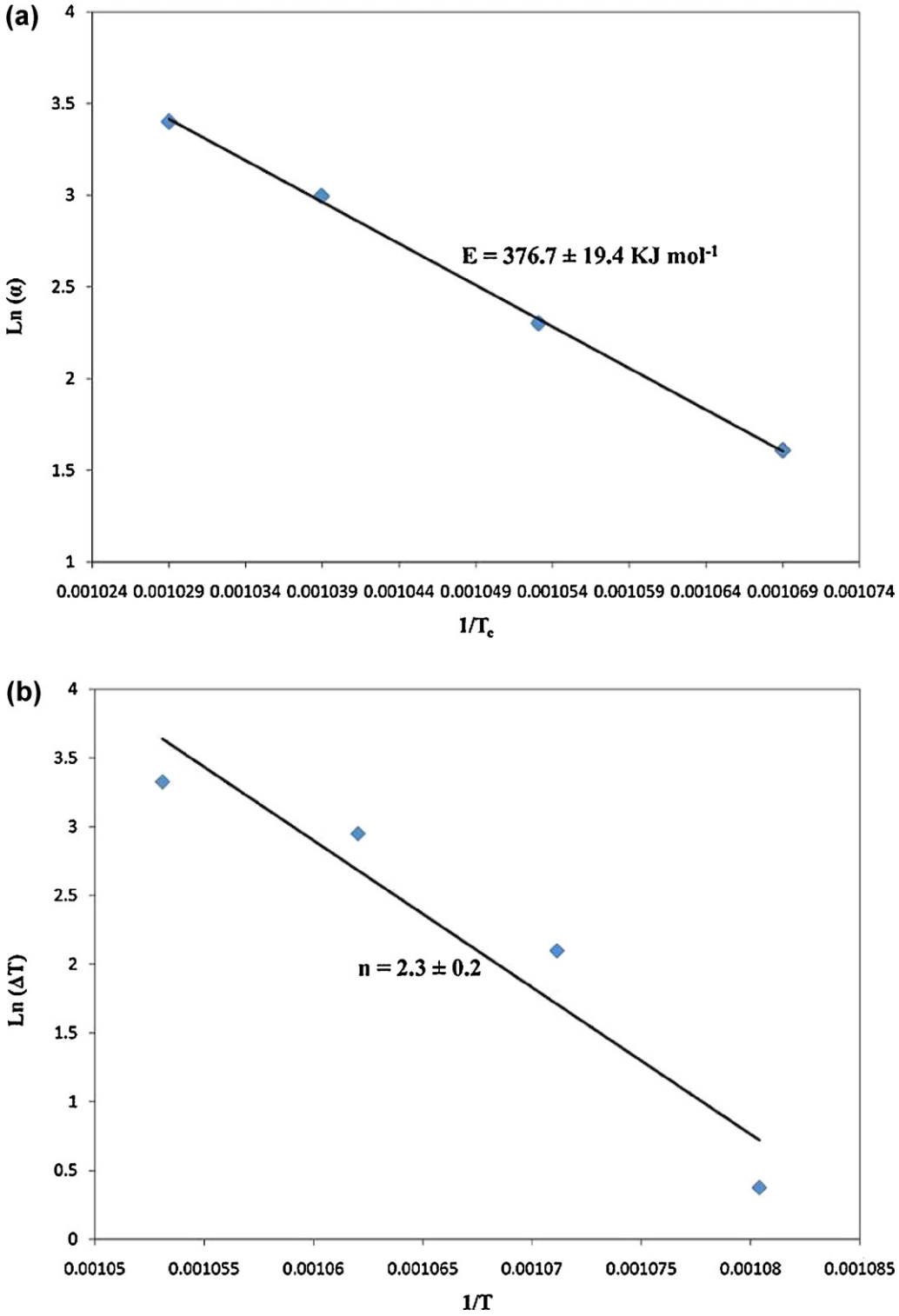

Fig. 7. (a) Variation of Ln (α) against $1/T$ to find the activation energy of the crystallization (regression fit $R^2 = 0.99$) and (b) variation of Ln (ΔT) against $1/T$ to find Avrami factor (regression fit $R^2 = 0.91$).

As Fig. 5 shows, the amorphous constituent of glass–ceramic is converted to the crystalline SiO_2 and along with decomposing of the mica, undesirable phases such as $Mg_7Si_8O_{22}(OH)_2$ are formed consequently with the increasing heating time. As such, it seems that any increasing heat treatment temperature from 700 °C leads to be instability of the mica through heating process.

According to the XRD analysis and Scherrer equation, the average crystallite size of mica was calculated as about 13 nm.

3.4. Microstructural investigation

Fig. 6(a) and (b) presents the TEM bright field image, corresponding to the selected area electron diffraction (SAED)

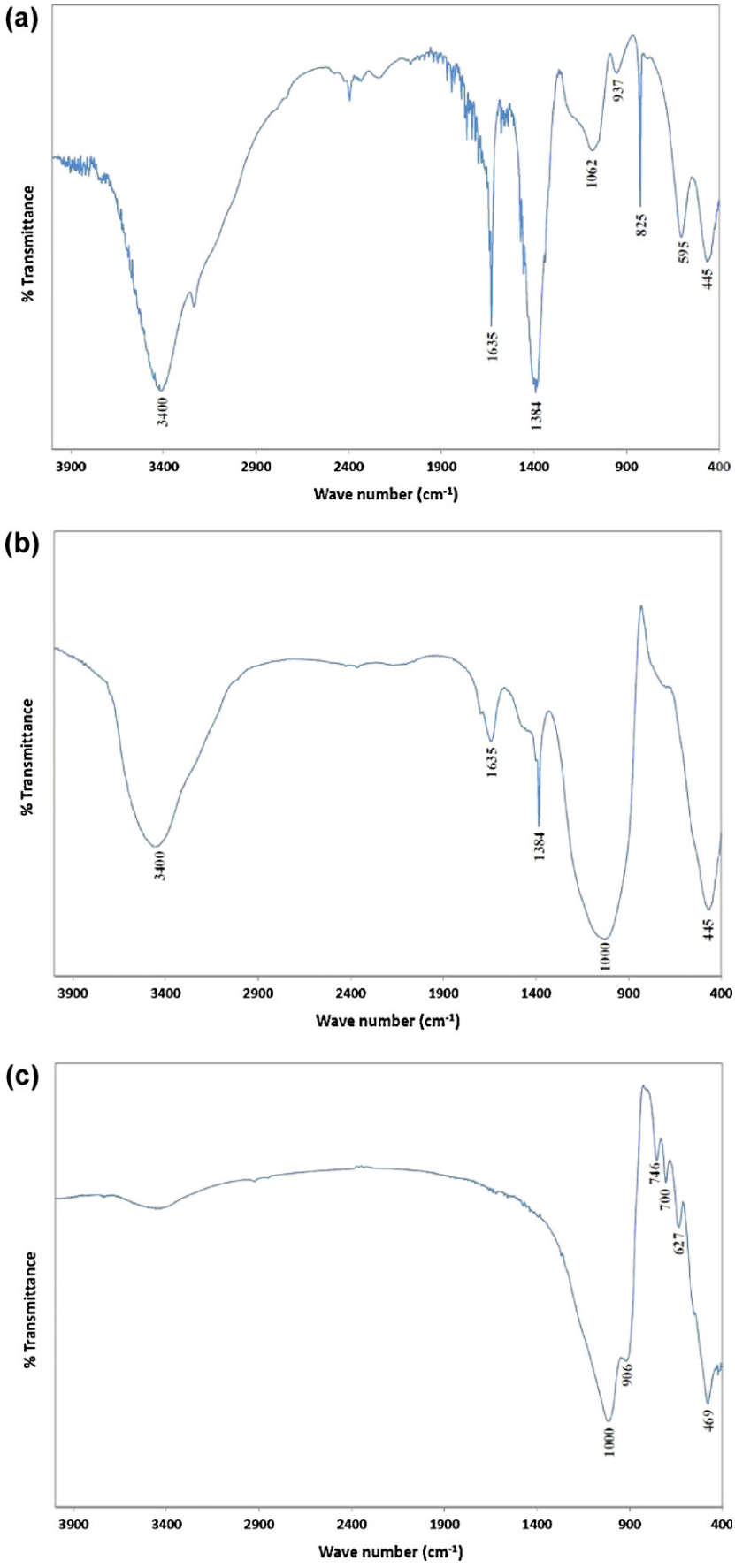

Fig. 8. IR spectra of various samples: (a) as-synthesized gel, (b) heat treated at 400 °C and (c) heat treated at 700 °C.

pattern and HRTEM image of the mica glass–ceramics heated at 700 °C for 4 h. The EDS spectra taken from the marked particle in Fig. 6(a) is also attached to the figure. The EDS spectrum indicates that the selected distinguished dark particle has the same composition as the mica phase composition. However, it is noticed that the trace of the lithium is not possible by the EDS microanalysis because it is a very light element ($Z = 3$) as well as the signal of Cu is due to the application of copper grid for supporting the sample. Fig. 6(b) shows the high resolution TEM (HRTEM) image of the proposed particle in Fig. 6(a). The mica nano-crystallite with the size of about 13 nm, which is seen in the micrograph, is in good agreement with those of the calculated value by means of the Scherrer formula. This is confirmed that the average crystallite size of mica synthesized via sol–gel process is smaller than the one prepared by conventional melted method and reported by Taruta et al. (<50 nm) [7].

3.5. Crystallization kinetics

The kinetic factors such as activation energy for crystallization and Avrami parameter were estimated through DSC diagrams using different heating rates with the same particle size distributions for all of the gels. This also according to the following equation was proposed by Marotta et al. [24,25]:

$$\mathrm{Ln}(\alpha) = \frac{-E}{RT_c} + C \quad (1)$$

$$\mathrm{Ln}(\Delta T) = \frac{-nE}{RT} + C \quad (2)$$

where α is the heating rate, E is the activation of energy for the crystallization, R is the ideal gas constant, T_c is the absolute temperature of crystallization peak, C is the constant, ΔT is the deviation from the baseline and n is the Avrami factor indicating the crystallization mechanism.

The activation energy of crystallization (E) and Avrami factor (n) were calculated by plotting the curves of Ln (α) and Ln (ΔT) versus $1/T$, respectively (Fig. 7(a) and (b)). Straight lines were fitted to the experimental data via regression analysis and the slope of any straight line was then obtained for estimating E and n values. So, the activation energy and Avrami factor values were obtained as 376.7 ± 19.4 kJ mol^{-1} and 2.3 ± 0.2, respectively.

According to the calculated n value, it seems that the crystallization behavior of the system is inclined to the bulk crystallization so that a combination of mono and two-dimensional growths of the crystals such as needle and flake like growths could be considered as predominant crystallization mechanisms for the system [24,25].

3.6. FTIR studies

Fig. 8 indicates that the Fourier transform infrared spectroscopy (FTIR) of the gel as well as the powders heat treated at 400 and 700 °C for 4 h. According to that, the detected IR broad peaks in the 2700–3600 cm^{-1} and 1635 cm^{-1} region are attributed to the stretching and bending vibration modes of υ_{O-H} and δ_{H-OH}, respectively [26]. The absorption peak around 1384 cm^{-1} is attributed to the presence of nitrate group in the xerogel [26]. It is observed that these peaks (related to OH and nitrites groups) reduce with the increasing temperature due to the evaporation and removal of these groups, hence, disappears in the heat treated sample at 700 °C. The IR band around 1000 cm^{-1} might be caused by the Si–O–Si formation and Si–O stretching mode [5]. It seems that this peak becomes stronger by increasing heat treatment which is related to the fixation of the ions in the three dimensional structure of the [SiO_4] with dehydration and removal of residual organic ions during the heat treatment. The IR bands at 627, 700 and 746 cm^{-1} may be attributed to the infrared vibration mode of alumino-silicate bonds due to the existence of lithium aluminum silicate which are appeared in the sample heat treated at 700 °C [27]. The peaks of about 440–470 cm^{-1} probably correspond to the deformation mode of Si–O–Si [26]. Finally, the absorption peak, around 906 cm^{-1} in the sample heat treated at 700 °C, can be corresponding to the alumino-silicate bond infrared vibration mode where the kind of the bond belongs to the mica structure [27]. This absorption peak confirms the formation of mica in the sample of heat treated at 700 °C.

4. Conclusions

The current research aims to synthesize a lithium–mica nano glass–ceramic via an aqueous sol–gel route. The obtained results can be summarized as follows:

(1) The mean crystallite size of mica was determined as 13 nm hence; it is smaller than the one synthesized by solid state method (<50 nm).
(2) Crystallization of the mica is derived from MgF_2 at 675 °C while, at next stages, there will occur the transformations of mica to norbergite and norbergite to chondrodite.
(3) According to the Marotta formula, the activation energy for crystallization and Avrami parameter are measured at 376.7 kJ mol^{-1} and 2.3, respectively. Based on this model it seems that the bulk crystallization along with the combination of a needle and flake like growths of the crystals is the predominant mechanism to describe the crystallization behavior of the sol–gel synthesized lithium–mica nano glass–ceramics.

References

[1] P.W. McMillan, Glass–Ceramics, second ed., Academic Press, London, 1979.
[2] M.C. Goncalves, L.F. Santos, R.M. Almeida, Rare-earth-doped transparent glass ceramics, C.R. Chimie 5 (2002) 845–854.
[3] G.H. Beall, L.R. Pinckney, Nanophase glass–ceramics, J. Am. Ceram. Soc. 82 (1999) 5–16.
[4] S. Taruta, T. Ichinose, T. Yamaguchi, K. Kitajima, Preparation of transparent lithium–mica glass–ceramics, J. Non-Cryst. Solids 352 (2006) 5556–5563.
[5] T. Hamasaki, K. Eguchi, Y. Koyanagi, A. Matsumoto, T. Utsunomiya, K. Koba, Preparation and characterization of machinable mica glass–ceramics by the sol–gel process, J. Am. Ceram. Soc. 71 (1988) 1120–1124.

[6] V.Saraswati, S. Raoot, Machinable mica-based glass–ceramic, J. Mater. Sci. 27 (1992) 429–432.
[7] S. Taruta, M. Suzuki, T. Yamakami, T. Yamaguchi, K. Kitajima, Preparation and ionic conductivity of transparent glass–ceramics containing a large quantity of lithium–mica, J. Non-Cryst. Solids 354 (2008) 848–855.
[8] S. Taruta, M. Matsuki, H. Nishikiori, T. Yamakami, T. Yamaguchi, K. Kitajima, Preparation and luminescent properties of Eu-doped transparent mica glass–ceramic, Ceram. Int. 36 (2010) 1303–1309.
[9] S. Taruta, M. Sakata, T. Yamaguchi, K. Kitajima, Crystallization process and some properties of novel transparent machinable calcium–mica glass–ceramics, Ceram. Int. 34 (2008) 75–79.
[10] X. Duan, D. Yuan, X. Cheng, Z. Sun, H. Sun, D. Xu, M. Lv, Spectroscopic properties of Co^{2+}:$ZnAl_2O_4$ nanocrystals in sol–gel derived glass–ceramics, J. Phys. Chem. Solids 64 (2003) 1021–1025.
[11] A. Tang, T. Hashimoto, H. Nasu, K. Kamiya, Sol–gel preparation and properties of TiO_2–P_2O_5 bulk glasses, Mater. Res. Bull. 40 (2005) 55–66.
[12] D.L. Li, L.B. Kong, L.Y. Zhang, X. Yao, Sol–gel preparation and characterization of transparent $KTiOPO_4$/SiO_2 nanocomposite glass for second harmonic generation, J. Non-Cryst. Solids 271 (2000) 45–55.
[13] Y.S. Chang, Y.H. Chang, I.G. Chen, G.J. Chen, Y.L. Chai, Synthesis and characterization of zinc titanate nano-crystal powders by sol–gel technique, J. Cryst. Growth 243 (2002) 319–326.
[14] M. Chatterjee, M.K. Naskar, Sol–gel synthesis of lithium aluminum silicate powders: the effect of silica source, Ceram. Int. 32 (2006) 623–632.
[15] J. Castillo, A.C. Yanes, J.J. Velazquez, J.M. Ramos, V.D. Rodriguez, Luminescent properties of Eu^{3+}–Tb^{3+}-doped SiO_2–SnO_2-based nano-glass–ceramics prepared by sol–gel method, J. Alloys Compd. 473 (2009) 571–575.
[16] C.F. Song, M.K. Lu, S.F. Wang, D. Xu, D.R. Yuan, Violet emission of Ce doped sol–gel Al_2O_3–SiO_2 glasses without any deoxidizing heat-treatment, Inorg. Chem. Commun. 7 (2004) 213–215.
[17] L. Xia, G.W. Wen, L. Song, X.Y. Wang, The effect of aluminum sources on synthesis of low expansion glass–ceramics in lithia–alumina–silica system by sol–gel route, J. Non-Cryst. Solids 355 (2009) 2349–2354.
[18] X. Duan, D. Yuan, X. Cheng, X. Wang, Optical absorption of Co^{2+} in gel-derived aluminosilicate glass–ceramics, Opt. Mater. 28 (2006) 1152–1155.
[19] L. Zhou, D. Chen, W. Luo, Y. Wang, Y. Yu, F. Liu, Transparent glass ceramic containing Er^{3+}:CaF_2 nano-crystals prepared by sol–gel method, Mater. Lett. 61 (2007) 3988–3990.
[20] X. Duan, D. Yuan, C. Luan, Z. Sun, D. Xu, M. Lv, Microstructural evolution of transparent glass–ceramics containing Co^{2+}:$MgAl_2O_4$ nanocrystals, J. Non-Cryst. Solids 328 (2003) 245–249.
[21] Y. Yu, Y. Wang, D. Chen, F. Liu, Efficient upconversion luminescence of Er^{3+}:SrF_2–SiO_2–Al_2O_3 sol–gel glass ceramics, Ceram. Int. 34 (2008) 2143–2146.
[22] S. Taruta, S. Shimodaira, T. Yamaguchi, K. Kitajima, New synthetic method and ionic conductivity of Na-4-mica, Mater. Lett. 60 (2006) 464–466.
[23] S.A. Hameed, A.M. Fathi, Preparation and characterization of silver nanoparticles within silicate glass ceramics via modification of ion exchange process, J. Alloys Compd. 498 (2010) 71–76.
[24] A. Marotta, A. Buri, F. Branda, Nucleation in glass and differential thermal analysis, J. Mater. Sci. 16 (1981) 341–344.
[25] A. Marotta, S. Saiello, F. Branda, A. Buri, Activation energy for the crystallization of glass from DDTA curves, J. Mater. Sci. 17 (1982) 105–108.
[26] N. Nallamuthu, I. Prakash, M. Venkateswarlu, S. Balasubramanyam, N. Satyanarayana, Sol–gel synthesis and characterization of Li_2O–As_2O_5–SiO_2 glassy system, Mater. Chem. Phys. 111 (2008) 24–28.
[27] K. Nakamoto, Infrared and Raman Spectra of Inorganic and Coordination Compounds, Wiley, New York, 1978.